Published in final edited form as:

Cell Rep. 2022 November 01; 41(5): 111574. doi:10.1016/j.celrep.2022.111574.

Disruption of mTORC1 rescues neuronal overgrowth and synapse function dysregulated by *Pten* loss

Kamran Tariq[1], **Erin Cullen**[2], **Stephanie A. Getz**[1], **Andie K.S. Conching**[1], **Andrew R. Goyette**[1], **Mackenzi L. Prina**[1], **Wei Wang**[1], **Meijie Li**[1], **Matthew C. Weston**[2,3,*], **Bryan W. Luikart**[1,3,4,*]

[1]Department of Molecular and Systems Biology, Geisel School of Medicine, Dartmouth College, Hanover, NH 03755, USA

[2]Department of Neurological Sciences, University of Vermont, Burlington, VT 05405, USA

[3]These authors contributed equally

[4]Lead contact

SUMMARY

Phosphatase and tensin homolog deleted on chromosome 10 (PTEN) is a negative regulator of AKT/mTOR signaling pathway. Mutations in PTEN are found in patients with autism, epilepsy, or macrocephaly. In mouse models, *Pten* loss results in neuronal hypertrophy, hyperexcitability, seizures, and ASD-like behaviors. The underlying molecular mechanisms of these phenotypes are not well delineated. We determined which of the *Pten* loss-driven aberrations in neuronal form and function are orchestrated by downstream mTOR complex 1 (mTORC1). Rapamycin-mediated inhibition of mTORC1 prevented increase in soma size, migration, spine density, and dendritic overgrowth in *Pten* knockout dentate gyrus granule neurons. Genetic knockout of *Raptor* to disrupt mTORC1 complex formation blocked *Pten* loss-mediated neuronal hypertrophy. Electrophysiological recordings revealed that genetic disruption of mTORC1 rescued *Pten* loss-mediated increase in excitatory synaptic transmission. We have identified an essential role for mTORC1 in orchestrating *Pten* loss-driven neuronal hypertrophy and synapse formation.

Graphical abstract

*Correspondence: matthew.c.weston@med.uvm.edu (M.C.W.), bryan.w.luikart@dartmouth.edu (B.W.L.).

AUTHOR CONTRIBUTIONS

M.C.W. and B.W.L. conceptualized the research; M.C.W., B.W.L., and K.T. obtained funding for the research. K.T., E.C., S.A.G., M.C.W., and B.W.L. designed experiments; K.T., E.C., S.A.G., A.K.S.C., A.R.G., and M.L.P. performed experiments; W.W. and M.L. generated tools and reagents; K.T., E.C., M.C.W., A.R.G., and M.L.P. analyzed the data; K.T., E.C., A.R.G., M.L.P., M.C.W., and B.W.L. wrote and edited the manuscript.

SUPPLEMENTAL INFORMATION

Supplemental information can be found online at https://doi.org/10.1016/j.celrep.2022.111574.

DECLARATION OF INTERESTS

Authors declare no competing interests.

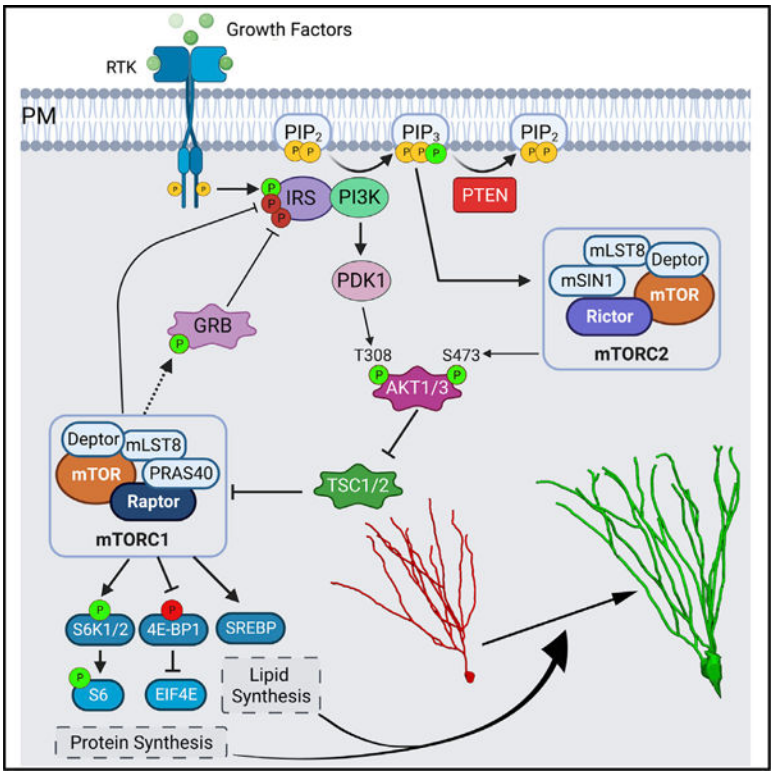

In brief

PTEN negatively regulates growth factor signaling through PI3K. Tariq et al. show that *Pten* loss in neurons causes overgrowth and increased excitatory synapse formation and function. Double knockout of *Raptor* and *Pten* normalizes neuronal growth, synapse number, and function. Neuronal hypertrophy and synapse formation downstream of PI3K requires mTORC1.

INTRODUCTION

Phosphatase and tensin homolog deleted on chromosome 10 (PTEN) is a dual specificity protein and lipid phosphatase that counteracts the activity of phosphoinositide 3-kinase (PI3K) by dephosphorylating phosphatidylinositol (3,4,5)-triphosphate (PIP_3) into phosphatidylinositol (4,5)-bisphosphate (PIP_2) (Tariq and Luikart, 2021). This negatively regulates the AKT (also known as protein kinase B)/mechanistic target of rapamycin (mTOR) signaling pathway (Waite and Eng, 2002). The AKT/mTOR pathway is an evolutionarily conserved signaling hub for regulating diverse cellular functions like growth, metabolism, proliferation, and survival (Laplante and Sabatini, 2009; Liu and Sabatini, 2020). Dysregulation of this signaling at key points has been implicated in multiple neurological disorders. In humans, mutations in *PTEN* gene have been linked with autism spectrum disorder (ASD), epilepsy, and macrocephaly (Conti et al., 2012; Klein et al., 2013; Satterstrom et al., 2020). In mouse models, loss of *Pten* has been shown to lead to neuronal hypertrophy, hyperexcitability, seizures, and ASD-like behaviors (Kwon et al., 2006; Luikart et al., 2011b; Skelton et al., 2020; Williams et al., 2015). Despite clear association between PTEN loss-mediated overactivation of AKT/mTOR signaling and aberrant neuronal form

and function, the precise downstream molecular mechanisms resulting in these varied phenotypes are not well delineated.

Currently, analogs of the naturally occurring mTOR inhibitor, rapamycin, are being investigated as a therapy for patients with ASD and tuberous sclerosis or PTEN hamartoma tumor syndrome (Cardamone et al., 2014; Mizuguchi et al., 2019; Sabatini et al., 1994). Biochemically, mTOR kinase forms two multi-protein complexes that share multiple proteins but also differ in two key proteins. mTOR complex 1 (mTORC1) selectively associates with regulatory associated protein of mTOR (RAPTOR), while mTOR complex 2 (mTORC2) selectively associates with rapamycin-insensitive companion of mTOR (RICTOR) (Sarbassov et al., 2005). mTORC1 is involved in the processes of protein translation, lipid synthesis, and autophagy, while mTORC2 is reported to regulate cytoskeletal organization (Angliker and Ruegg, 2013; Huang et al., 2013; Laplante and Sabatini, 2009, 2012). However, complexity of the signaling pathway leaves room for cross talk and feedback among the effectors of two mTOR complexes (Liu and Sabatini, 2020). Rapamycin is canonically thought to inhibit hyperactivity of AKT/mTOR pathway by inhibiting the formation of mTORC1 only (Getz et al., 2016; Kang et al., 2013). Rapamycin has been shown to prevent neuronal aberrations in mouse models of *Pten* loss as well (Getz et al., 2016; Weston et al., 2012). However, some studies have revealed that chronic treatment with rapamycin may also result in inhibition of mTORC2 activity (Sarbassov et al., 2006). There is now evidence that disruption of mTORC2 by targeting *Rictor* can correct seizures and behavioral phenotypes associated with *Pten* deficiency (Chen et al., 2019). Thus, it is unclear which of the *Pten* loss-mediated phenotypes are orchestrated specifically by mTORC1.

Here, we determine that mTORC1 is necessary for PTEN loss-mediated neuronal hypertrophy and synapse formation. To examine this, we first utilized treatment with rapamycin to pharmacologically inhibit mTORC1 in retrovirus-infected granule neurons with *Pten* loss *in vivo*. We found that rapamycin treatment was able to prevent *Pten* loss-mediated increase in soma size, ectopic migration, spine density, and dendritic overgrowth. To confirm that this was a result of inhibition of mTORC1 only, and not mTORC2, we genetically knocked out *Raptor* in addition to *Pten*. We found that genetic disruption of mTORC1 was sufficient to rescue the parameters of neuronal hypertrophy *in vivo*, as well as *in vitro*. To determine if the rescue of neuronal morphology also resulted into a functional rescue, we employed electrophysiology, which showed that genetic disruption of mTORC1 rescued *Pten* loss-mediated increase in excitatory synaptic transmission *in vitro*. Thus, our data show that mTORC1 is necessary for *Pten* loss-mediated increases in neuronal growth and synaptic function.

RESULTS

Rapamycin treatment rescues *Pten* loss-mediated neuronal hypertrophy

At postnatal day 7 (P7), $Pten^{flx/flx}$ animals were co-injected into the dentate gyrus with a retrovirus encoding a fluorophore (mCherry) with a downstream Cre, and a control retrovirus with just a fluorophore (GFP) and no Cre (Figure 1A). The specificity of this experimental approach in targeting newborn granule neurons for genetic manipulation has

been described previously (Fricano-Kugler et al., 2016; Williams et al., 2015). Here, the mCherry-expressing newborn granule neurons are knocked out for their respective flox genes (notated as Cre+ neurons in the figures), while GFP-expressing neurons serve as their in-tissue wild-type (WT) controls (notated as Cre− neurons in the figures). Vehicle or rapamycin (10mg/kg of body weight) was injected intraperitoneally from P10 to P31 daily. Immunohistochemical analysis revealed that rapamycin treatment significantly rescued the greater soma size of vehicle-treated *Pten* KO granule neurons (Table S1A and Figures 1B and 1C). The migration of granule neurons was quantified as a percentage of distance travelled through granule cell layer (GCL), with hilar boundary as a starting baseline. The significantly farther migration of vehicle-treated *Pten* KO neurons along the GCL was also rescued by rapamycin treatment (Table S1B and Figures 1B and 1D). Additionally, rapamycin treatment rescued the increased spine density of vehicle-treated *Pten* KO neurons in middle molecular layer (Table S1C and Figures 1E and 1F). These data suggest that *Pten* loss-mediated neuronal hypertrophy can be rescued by rapamycin treatment.

Rapamycin treatment rescues *Pten* loss-mediated dendritic overgrowth

We next investigated the effect of rapamycin treatment on *Pten* KO-mediated dendritic overgrowth. Vehicle or rapamycin (10 mg/kg of body weight) was administered intraperitoneally to $Pten^{flx/flx}$ animals daily from P10 to P31. Retrovirally infected and immunolabeled granule neurons were reconstructed, and their dendritic arbor was analyzed. Sholl analysis revealed that vehicle-treated *Pten* KO neurons had an increased number of intersections compared with WT control neurons. This increase was completely rescued in rapamycin-treated *Pten* KO neurons (Table S1D and Figures 2A–2C). The total dendritic length was also increased in vehicle-treated *Pten* KO neurons, which was rescued by rapamycin treatment (Table S1E and Figures 1A, 1B, and 1D). Further analysis revealed that vehicle-treated *Pten* KO neurons have more primary dendrites protruding directly out of the soma compared with their WT control. This increase in number of primary dendrites was also completely rescued with rapamycin treatment (Table S4 and Figure S1A). The *Pten* KO-mediated increase in number of branch points (nodes) and endpoints of vehicle-treated neurons was also rescued in rapamycin-treated *Pten* KO neurons (Tables S4B and S4C and Figures S1B and S1C). The effect of rapamycin on dendritic growth was also reflected in the Sholl analysis of dendrite length (Table S4D and Figure S1D).

Genetic disruption of mTORC1 rescues *Pten* loss-mediated neuronal hypertrophy

The above results suggest that rapamycin effectively rescues several morphological alterations caused by *Pten* loss. In addition, previously published results suggest that rapamycin rescues the electrophysiological effects of *Pten* loss (Weston et al., 2012). The mTORC1 complex is thought to be the primary target of rapamycin; however, rapamycin may also inhibit mTORC2 and other targets (Karalis et al., 2022). We therefore tested whether the rescue of *Pten* KO phenotype observed with rapamycin treatment was mTORC1 specific. To do this, $Pten^{flx/flx}Raptor^{flx/flx}$ animals were generated to genetically knock out *Raptor* resulting in disruption of mTORC1. The $Raptor^{flx}$ allele has been validated, and we and others have demonstrated the effect of *Raptor* deletion on neuronal and synaptic development (Godale et al., 2022; McCabe et al., 2020; Sengupta et al., 2010). At P7, $Pten^{flx/flx}$ and $Pten^{flx/flx}Raptor^{flx/flx}$ animals were co-injected into the dentate

gyrus with a retrovirus encoding a fluorophore (GFP) with a downstream Cre, and a control retrovirus with just a fluorophore (mCherry) and no Cre (Figure 3A). Here, the GFP-expressing newborn granule neurons are KOs for their respective flox genes, while mCherry-expressing neurons serve as their in-tissue WT controls. To investigate the role of mTORC1 in development of *Pten* KO-mediated somal hypertrophy, we quantified soma size of retrovirally infected immunolabeled granule neurons at P28. We observed that *Pten* KO neurons had significantly greater soma size when compared with their WT control. This increase in soma size was completely rescued in *Pten* and *Raptor* double knockout (DKO) neurons (Table S1A and Figures 3B and 3D). We further examined the role of mTORC1 in aberrant migration of *Pten* KO granule neurons. The *Pten* KO neurons migrate significantly farther from the hilus along the GCL, when compared with their WT control. This farther migration was completely rescued in *Pten* and *Raptor* DKO neurons (Table S1B and Figures 3B and 3E). The dendritic spine density was also found to be significantly increased in *Pten* KO neurons. This increase in number of spines in middle molecular layer was reduced to WT density in *Pten* and *Raptor* DKO neurons (Table S1C and Figures 3C and 3F). Additionally, the decrease in spine head diameter seen in *Pten* KO neurons was rescued in *Pten* and *Raptor* DKO neurons (Table S1D). However, the increased spine length of *Pten* KO neurons persisted in the *Pten* and *Raptor* DKO neurons (Table S1E). These data suggest that *Pten* loss-mediated neuronal hypertrophy can be rescued by targeting *Raptor* to disrupt mTORC1.

Genetic disruption of mTORC1 rescues *Pten* loss-mediated dendritic overgrowth

To examine the role of mTORC1 in the *Pten* loss-mediated dendritic overgrowth of granule neurons, we reconstructed and quantified retrovirally infected immunolabeled *Pten* KO granule neurons, as well as *Pten* and *Raptor* DKO granule neurons at P28 (Figures 4A and 4B). We observed that *Pten* KO granule neurons had more elaborate dendritic arbor. Sholl analysis revealed that *Pten* KO neurons had an increased number of intersections, when compared with WT control neurons. This increase was completely rescued in *Pten* and *Raptor* DKO neurons (Table S1F and Figure 4C). The total dendritic length was also increased in *Pten* KO neurons, which was rescued in *Pten* and *Raptor* DKO neurons (Table S1G and Figure 4D). Further analysis revealed that *Pten* KO neurons have more primary dendrites protruding directly out of the soma, when compared with their WT control. This increase in number of primary dendrites was completely rescued in *Pten* and *Raptor* DKO neurons (Table S4A and Figure S2A). The *Pten* KO-mediated increase in number of branch points (nodes) and endpoints was also rescued in *Pten* and *Raptor* DKO neurons (Tables S4B and S4C and Figures S2B and S2C). *Pten* and *Raptor* DKO also rescued the *Pten* KO-mediated increase in Sholl of length (Table S1D and Figure S2D). These data suggest that mTORC1 plays an important role in the development of *Pten* loss-mediated dendritic overgrowth, which can be rescued by targeting *Raptor* to disrupt mTORC1.

The rescue of *Pten* loss-mediated dendritic overgrowth by genetic KO of *Raptor* complements the similar rescue observed by pharmacological inhibition of mTORC1 and points toward an integral role of mTORC1 in the development of dendritic overgrowth.

Genetic disruption of mTORC1 results in rescue of neuronal morphology caused by PTEN loss in single neuron cultures

In addition to morphological alterations, we and others have previously shown that *Pten* loss leads to alterations in membrane excitability and excitatory synaptic transmission, both pre- and postsynaptic. To test whether these changes were dependent on mTORC1 signaling, we made single neuron cultures of hippocampal neurons from P0–P1 $Pten^{flx/flx}$ and $Pten^{flx/flx}Raptor^{flx/flx}$ animals on astrocytes isolated from P0–P1 WT mice. At the time of plating, we transduced the neurons with adeno-associated viruses expressing either an mCherry-Cre fusion protein or mCherry alone, both driven by the SYN promoter, to generate knockout (*Pten* KO or *PtenRaptor* KO) or control neurons, respectively. Previously, we showed that this strategy strongly reduces both the PTEN and RAPTOR protein levels.

First, we tested whether, as seen in the granule neuron experiments, the morphological effects of *Pten* loss were rescued by mTORC1 inactivation in this experimental preparation (Figure 5). Soma area, total dendritic length, and the number of excitatory synapses per neuron (as assayed by the number of VGLUT puncta) were all increased by *Pten* KO (Figures 5A and 5B). Similar to the data from newborn granule neurons, soma area and dendritic length were rescued in *PtenRaptor* DKO neurons. The mean number of excitatory synapses was increased by *Pten* KO and decreased in *PtenRaptor* DKO neurons, although not significantly.

Next, we whole-cell patch-clamped the neurons and performed current-clamp analysis of intrinsic membrane properties (Figure 5C and Table S2). Input resistance and capacitance were decreased and increased by *Pten* KO, respectively, and rescued by *PtenRaptor* DKO, as expected from the changes in morphology. Taken together, these data suggest that the morphological changes caused by PTEN loss are similar in newborn granule neurons and cultured hippocampal neurons, and that these changes are rescued by decreasing mTORC1 activity in both model systems.

Genetic disruption of mTORC1 rescues *Pten* loss-mediated increases in excitatory synaptic transmission

Previously we showed, in both newborn granule neurons and cultured hippocampal neurons, that *Pten* loss increased the strength of excitatory neurotransmission. To test whether mTORC1 inhibition rescued this increase, we first evoked EPSCs (eEPSCs) and measured their peak amplitude. eEPSC amplitude was increased by *Pten* loss and rescued in *PtenRaptor* DKO neurons (Figure 6A), indicating that the increase in excitatory neurotransmission caused by *Pten* loss is mTORC1 dependent.

The observed increase in eEPSCs following *Pten* loss could be due to changes in the amplitude of the postsynaptic response to single SV fusion (quantal size) or the number of fusion-competent SVs (readily releasable pool, RRP). First, to test for changes in quantal size, we recorded miniature EPSCs (mEPSCs) and measured their amplitude and decay time constants (Figure 6B), properties that are primarily dictated by postsynaptic ionotropic receptor levels and/or activity. In line with our previous observations in multiple cell types,

the mEPSC peak amplitude was increased by PTEN loss, by about 20%. This increase was also rescued in *PtenRaptor* DKO neurons (Figure 6B).

Next, we assessed the number of SVs in the RRP following *Pten* loss, which can be directly quantified in a single neuron by applying a pulse of hypertonic sucrose (500 mM) to induce the exocytosis of all of a neuron's fusion-competent vesicles (Rosenmund and Stevens, 1996). The integral of the transient current during sucrose application represents the total charge contained in the RRP (RRP_{suc}), and the total number of vesicles in the RRP can then be calculated by dividing the total charge by the average charge of the miniature events from each neuron. We found that RRP_{suc} in glutamatergic *Pten* KO neurons was increased compared with that of control neurons, and that this increase was rescued by *PtenRaptor* DKO. As a result, the mean number of SVs contained in the RRP_{suc} of *Pten* KO glutamatergic neurons was increased by almost 40% relative to that of control neurons, and that this increase was rescued by mTORC1 inhibition (Figure 6C). In agreement with the changes in synapse (Figure $5B_3$) and SV number (Figure 6C), the mEPSC frequency was increased by *Pten* KO and rescued by *PtenRaptor* DKO (Figure 6D). We also assessed potential changes in SV release, as we previously showed that mTORC2 activity is required to maintain normal SV release efficiency. However, in agreement with the conclusion that the primary effects of *Pten* loss are mediated by mTORC1, we did not observe any difference in SV release probability in *Pten* KO or *PtenRaptor* DKO neurons (Figures 6E and 6F).

The activation of mTORC1 leads to S6 Kinase-mediated phosphorylation of downstream S6 protein (S6) at S235/236 residue (Antion et al., 2008). To investigate whether the KO of *Raptor* leads to disruption of mTORC1 complex and subsequently its activity, phosphorylation of S6 protein (pS6) was used as a measure of activity of mTORC1. Immunohistochemical analysis at P28 revealed that *Pten* KO neurons have an elevated pS6 fluorescence intensity relative to their in-tissue WT controls, indicating increased mTORC1 activity. However, this elevation in pS6 intensity was completely rescued in *Pten* and *Raptor* DKO neurons when compared with their in-tissue WT controls, indicating successful disruption of mTORC1 complex resulting in a loss of its activity (Table S3A and Figures 7A and 7B). Knockout of *Pten* resulted in an increase in the phosphorylation of AKT Thr308. The *Pten*/*Raptor* DKO displayed a greater increase than seen in the single KO (Table S3B and Figures 7C and 7D). Loss of *Pten* also increased the phosphorylation of the mTORC2 target, AKT Ser473, and this increase was even greater in the DKO (Table S3C and Figures 7E and 7F). Together these results demonstrate that *Pten* loss drives downstream activity of both mTORC1 (pS6) and mTORC2 (pAKT Ser473). Knockout of *Raptor* in conjunction with *Pten* results in feedback causing an increase in both pAKT Thr308 and pAKT Ser473.

DISCUSSION

PTEN loss-mediated aberrations in neuronal form and function are implicated in neurological disorders like ASD and epilepsy (Conti et al., 2012). In dentate gyrus granule neurons, pharmacological inhibition of mTORC1 by rapamycin treatment prevented *Pten* loss-mediated increase in soma size, ectopic migration, spine density, and dendritic overgrowth. These data confirm and extend previous work on rapamycin rescue in *Pten* KO

models (Zhou et al., 2009; Zhu et al., 2012). Postnatal genetic knockout of *Raptor* also confirmed that the disruption of mTORC1 was sufficient to block neuronal hypertrophy after *Pten* deletion *in vivo*, as well as in single neuronal cultures. Electrophysiological recordings from cultured neurons revealed that genetic disruption of mTORC1 by knocking out *Raptor* rescued *Pten* loss-mediated increase in excitatory synaptic transmission as well. Here, we determine the contribution of downstream mTORC1 activity on a comprehensive set of morphological and physiological measurements in *Pten* KO neurons. Taken together, our data indicate that mTORC1 is necessary for neuronal growth and synapse formation caused by PTEN dysfunction.

For proper neuronal development and synaptic connectivity, neurons must integrate extracellular signals to guide their dendritic growth, form specialized structures like spines and synapses for communication, and retract and eliminate some of these connections to adapt the neuronal circuitry to changing environmental cues. mTORC1 is implicated in these processes through its regulation of protein synthesis, lipid metabolism, and autophagy via its downstream effectors (Saxton and Sabatini, 2017). mTORC1 regulates biosynthesis of mRNA and ribosomes by activating S6 kinase. Activation of mTORC1 also inhibits 4E-BP1 to relieve its suppression of EIF4E, which upregulates cap-dependent protein translation (Laplante and Sabatini, 2009). In addition, mTORC1 activates sterol regulatory element binding protein to drive biosynthesis of lipids (Takei and Nawa, 2014). Activation of mTORC1 also inhibits the process of autophagy and lysosome biogenesis under nutrient-rich conditions (Dunlop and Tee, 2014). Thus, mTORC1 activation supplies protein and lipid components for overall anabolic cell growth, while putting brakes on catabolic processes of cell death. Importantly, for highly specialized neurons that have diverse shapes and properties, the activity of mTORC1 is also spatially regulated. mTORC1 has been shown to localize in dendritic compartments and respond to local signals like brain-derived neurotrophic factor and neurotransmitters to orchestrate synaptic plasticity through its effectors (Takei et al., 2004). Further, dynamic regulation of mTOR signaling is reported to be required for activity-dependent sculpting of neuronal arbor of developing neurons only (Skelton et al., 2020). Similarly, rapamycin-mediated pharmacological inhibition of mTORC1 also rescues the neuronal alterations associated with hyperactivation of mTORC1 signaling but requires an early intervention before such alterations are fully established, which may not be possible clinically because of late diagnosis window in patients (Getz et al., 2016).

The present study indicates that *Pten* knockout in neurons drives the mTORC1 pathway by phosphorylation of AKT Thr308(305). In cancer, this occurs via PIP_3 recruitment of the AKT PH domain and phosphorylation by PDK1 (Peterson et al., 2009). Additionally, after *Pten* deletion, we observe mTORC2 activation as indicated by increased AKT Ser473(472) phosphorylation. In cell lines, mSIN1 is recruited by PIP_3 to release inhibition of mTORC2 and phosphorylate AKT Ser473 (Liu et al., 2015). After *Raptor* deletion, we note pS6 Ser 235/236 returns to baseline, while there are even greater levels of pAKT Thr308 and Ser473. This supports the existence of feedback from mTORC1 loss to upstream GRB and IRS proteins driving increased PI3K activity (Hsu et al., 2011; Tzatsos, 2009). That *Raptor* deletion results in WT levels of pS6 with increased pAKT Ser473, demonstrating the ablation of mTORC1 function while leaving mTORC2 function in-tact. Thus, our data

demonstrate that activation of mTORC1 is necessary to drive increased neuronal migration, somal hypertrophy, dendrite growth and branching, dendrite spine formation, and synapse formation that results from *Pten* loss.

There are many cellular changes associated with PTEN knockout that could contribute to ASD or epilepsy that the current study does not examine. The loss of PTEN has been associated with altered numbers of inhibitory neurons (Vogt et al., 2015) and changes in glial numbers (Chen et al., 2015; Sarn et al., 2021). Changes in action potential kinetics and burst firing have also been seen in *Pten* KO neurons (Santos et al., 2017; Williams et al., 2015). *Pten* KO also results in inappropriate synapse formation between cells that are not coupled in the WT mice (Skelton et al., 2019). While the current study indicates that mTOR disruption can rescue overgrowth and synapse number, future studies will be necessary to address changes in cell division, differentiation, excitability, and synapse specificity. There are signaling intermediates upstream of mTORC1 including PIP_3/PIP_2, AKT, and mTORC2, whose direct effects on *Pten* loss-mediated neuronal alterations remain to be uncovered.

Studies on *Pten* loss-driven alterations in neuronal form and function have mainly focused on overactivation of mTORC1. However, chronic treatment with rapamycin has been shown to inhibit mTORC2, which hints toward a possible role of mTORC2 inhibition in rescuing *Pten* loss phenotype (Sarbassov et al., 2006). *Rictor*, but not *Raptor*, loss has been shown to prevent seizures and behavioral changes in $Pten^{flx/flx}$ x CamKIIα-Cre mice (Chen et al., 2019). In contrast, we find that *Raptor* loss rescues autonomous effects on neuronal morphology and synapse formation and function. This is consistent with the effect of *Raptor* loss in animal models of Tuberous Sclerosis Complex disorder (Karalis et al., 2022). It is unknown what cellular changes give rise to emergent behavioral changes. However, we have hypothesized that the increased growth and associated increase in inappropriate excitatory contacts underlie the symptoms of ASD. Further studies are needed to reconcile these seemingly incongruent findings and to tease apart the role of individual mTOR complexes in development of these nuanced *Pten* loss phenotypes. To summarize, using both pharmacological inhibition and genetic knockout approaches in this study, we identify an essential role for mTORC1 in mediating *Pten* loss-mediated neuronal hypertrophy and excitatory synaptic formation and function *in vivo* and *in vitro*.

Limitations of the study

This study examines the effect of mTORC1 loss on *Pten* knockout neurons on a single-cell basis *in vivo* and *in vitro*. As such, this study largely captures cell-autonomous gene functions and is unable to detect emergent non-autonomous effects that may occur in tissues with widespread gene deletion and complicated intercellular interactions. The virus-based system to target single cells *in vivo* does not lend itself to standard biochemical methods to study intracellular signaling. Thus, this study relies on antibodies displaying specific staining using histology to elucidate intracellular signaling changes. *In vitro* systems allow us to assay synapse formation and function but do not recapitulate the architecture of synaptic connectivity generated *in vivo*. Finally, the limited number of cells that are infected *in vivo*, and *in vitro* strategies, do not lend themselves to studying the impact of genetic manipulation on emergent animal behaviors. We do not know if autonomous

neuronal changes result in emergent behavioral changes reminiscent of ASD or whether such changes must be compounded by phenotypes in other cell types such stem cells and glia or compounded by the interaction of multiple aberrant cell types.

STAR★METHODS

RESOURCE AVAILABILITY

Lead contact—Further information and requests for resources and reagents should be directed to and will be fulfilled by the lead contact, Bryan Luikart (Bryan.W.Luikart@Dartmouth.edu).

Materials availability

- All mice and viral constructs used in this study have been previously generated and are all available through Addgene or Jackson laboratories with individual catalog numbers for each item listed in the key resources table and the subsections below.

Data and code availability

- NeuroLucida neuronal reconstruction data have been deposited at Neuromorpho.org and are publicly available as of the date of publication. Other data reported in this study consist of image stacks, ROIsets for image analysis, spreadsheets for quantitative image analysis and electrophysiology traces for which no standard repositories exist. To request access, contact the lead contact.
- This paper does not report original code.
- Any of these data or additional information required to reanalyze the data reported in this paper is available from the lead contact upon request.

EXPERIMENTAL MODEL AND SUBJECT DETAILS

Animals—All procedures were approved by Dartmouth College's or the University of Vermont's Institutional Animal Care and Use Committee (IACUC) and Association for Assessment and Accreditation of Laboratory Animal Care Review Board. *Pten*$^{flx/flx}$ animals (B6.129S4-*Pten*^{tm1Hwu}/J with C57BL/6J background from Jackson Laboratory) were crossed with *Raptor*$^{flx/flx}$ animals (Jackson Labs stock: 013188) to generate *Pten*$^{flx/flx}$*Raptor*$^{flx/flx}$ animals. Animals were placed on a 12-hour light/dark cycle with chow and water provided *ad libitum*. Animals of either sex were utilized for these experiments; because sex does not interact with neuronal hypertrophy of *Pten* knockout neurons, sex was not statistically isolated as a biological variable (Santos et al., 2017).

Single neuron cultures—Single-neuron primary cultures from *Pten*$^{flx/flx}$, *Raptor*$^{flx/flx}$, *Pten*$^{flx/flx}$*Raptor*$^{flx/flx}$ were derived from P0 animals of both sexes were grown on astrocytes derived from WT C57BL/6J mice (Jackson Labs stock: 000664).

METHODS DETAILS

Viral constructs—Retroviral constructs containing GFP or mCherry, with or without Cre recombinase (Addgene # 66692, 66693, 66696, and 66700) were generated and packaged as previously described (Luikart et al., 2011a; Williams et al., 2015).

Surgery—The detailed method of stereotaxic surgery has been published previously (Fricano-Kugler et al., 2016). Briefly, isoflurane-anesthetized pups at postnatal (P) day 7 were injected with 2mL of replication-incompetent retroviruses into the hippocampal dentate gyrus of both hemispheres (coordinates relative to lambda: x = ±1.3mm, y = +1.55mm, z = −2.3 to −2.0mm), at the rate of 0.3μL/min with 25% of the virus injected at each z-depth. At P21 or P28, animals were anesthetized with Avertin (Sigma Aldrich) and trans-cardially perfused with 4% paraformaldehyde (PFA) in phosphate-buffered saline (PBS) containing 4% sucrose for fixation (IHC).

Rapamycin treatment—Mice received daily intraperitoneal (IP) injections of either rapamycin (10mg/kg of body weight; Cayman Chemical), or vehicle from P10–31. A 25 mg/mL stock solution of rapamycin was made in ethanol. A working stock solution of 1 mg/mL concentration was prepared fresh daily with 4% rapamycin or ethanol (for vehicle group), 5% Tween80 (Fisher Biosciences), and 5% PEG400 (Sigma Aldrich) (Getz et al., 2016). The mice were perfused the day after final rapamycin/vehicle treatment.

Immunohistochemistry (IHC)—The coronal brain slices of 50μm or 150μm thickness were cut using a vibratome (Leica VT1000 S). These slices were permeabilized with PBS containing 0.4% Triton X-(PBST) for 30 min and blocked with PBS containing 10% donor horse serum (DHS) for 1 h at room temperature. Sections were incubated with primary antibodies (Chicken anti-GFP, 1:3000, abcam#13970; Rabbit anti-mCherry, 1:3000, abcam#167453; Mouse anti-mCherry, 1:3000, TaKaRa#632543; Rabbit anti-phospho-S6 S235/236, 1:200, Cell Signaling#4858; Rabbit anti-phospho-AKT-Thr308, 1:100, cell signaling#13038; Rabbit anti-phospho-AKT-Ser473, 1:100, Cell Signaling#9271) for 48 h at 4°C in PBS with 2.5% DHS. After three 15 min washes with PBST, sections were incubated for 48 h at 4°C with secondary antibodies (Alexa Fluor 488 conjugated goat anti-chicken IgG, Jackson ImmunoResearch Labs#103-545-155; Cy3 conjugated donkey anti-rabbit IgG, Jackson ImmunoResearch Labs#711-165-152; Cy3 conjugated donkey anti-mouse IgG, Jackson ImmunoResearch Labs#715-165-150; Alexa Fluor 647 conjugated goat anti-rabbit IgG, Jackson ImmunoResearch Labs#111-605-144) at a concentration of 1:200 in PBS containing 2% DHS. After three 15 min washes with PBST, sections were mounted in Vectashield (H-1000, Vector Laboratories) on glass slides.

Microscopy and image analysis—For morphological analysis, images were acquired using LSM510 laser-scanning confocal microscope (Zeiss, Germany). For soma size and migration analysis, z-stacks of supra- and infrapyramidal blades of dentate gyrus were acquired at 40×/1.3 μm oil immersion lens with 0.7× zoom, at 512 × 512 resolution with 2 μm z-step. Soma size was quantified by circling somas at maximum circumference using ImageJ/Fiji software (NIH) as described previously (Fricano et al., 2014). Migration was expressed as a percentage of granular cell layer (GCL) travelled, by dividing the distance

of soma from hilus boundary by total local GCL width (Getz et al., 2016; Perederiy et al., 2013). Z-stacks of spines were acquired at 63×/1.3 μm oil immersion lens with 3× zoom, at 512 × 512 resolution with 0.5 μm z-step. After deconvolution (Sage et al., 2017) using ImageJ/Fiji, dendritic spine density was quantified with Neuron Studio software (Rodriguez et al., 2008) as described previously (Williams et al., 2015). For dendritic arbor analysis, images of dentate gyrus were acquired at 20×/0.75μm plan-apochromat lens with 1× zoom, at 512 × 512 resolution with 2 μm z-step. Neurons were reconstructed in 2D or 3D by user-guided semi-automated tracing in Neurolucida360 (MBF Biosciences) software. Branched structure and Sholl analysis were performed in Neurolucida Explorer (MBF Biosciences) software.

Single neuron cultures—Single-neuron primary cultures were grown on astrocytes derived from WT C57BL/6J mice (Jackson Labs stock: 000664). Cortices were dissected from postnatal day 0–1 (P0-P1) mice of either sex and placed in 0.05% trypsin-EDTA (Gibco) for 15 min at 37°C ina Thermomixer (Eppendorf) with gentle agitation (800 rpm). Then, the cortices were mechanically dissociated with a 1 mL pipette tip and the cells were plated into T-75 flasks containing astrocyte media [DMEM media supplemented with glutamine (Gibco) and MITO + Serum Extender (Corning). After the astrocytes reached confluency, they were washed with PBS (Gibco) and incubated for 5 min in 0.05% trypsin-EDTA at 37°C, and then resuspended in astrocyte media. The astrocytes were added to 6-well plates containing 25-mm coverslips precoated with agarose-coated coverslips stamped with coating mixture [0.7 mg/mL collagen I (Corning) and 0.1 mg/mL poly-D-lysine (Sigma) in 10 mM acetic acid] using a custom-built stamp to achieve uniformly sized, astrocyte microislands (200-μm diameter).

Hippocampi from P0-P1 mice of both sexes were dissected in cold HBSS (Gibco), digested with papain (Worthington) for 60–75 min, and treated with inactivating solution (Worthington) for 10 min, both while shaking at 800 rpm at 37°C in a Thermomixer. The neurons were then mechanically dissociated and counted. 2000–3000 neurons/well were added to 6-well plates in NBA plus [Neurobasal-A medium (Gibco) supplemented with Glutamax (Gibco) and B27 (Invitrogen)], each well containing a 25-mm coverslip with astrocyte microislands. After plating, approximately 4×10^{10} genome copies (GC) of either AAV8-SYN-mCherry-Cre or AAV8-SYN-mCherry virus (UNC Vector Core) was added to each well.

Single neuron histology—Neurons were rinsed three times with PBS, fixed with 4% PFA for 30 min, and then washed with PBS three times. Neurons were then placed in blocking solution (10% NGS, 0.1% Triton X-100, and PBS) at room temperature for 1 h. The following primary antibodies in blocking solution were then applied to the neurons at 4°C overnight: MAP2 (mouse monoclonal, 1:1000 dilution, Synaptic Systems, Cat# 188 011, RRID:AB_2147096) and VGLUT1 (rabbit polyclonal, 1:5000 dilution, Synaptic Systems, Cat # 135 302, RRID:AB_887877. Following primary antibody application, cells were washed three times in PBS and then incubated in the following Alexa Fluor secondary antibodies (Invitrogen/Molecular Probes) for 1 h at room temperature: goat anti-mouse 488 (1:1000, Cat # A-11017, RRID:AB_143160) and goat anti-rabbit 647 (1:1000,

Cat# A-21244, RRID:AB_141663). Cells were then mounted to slides with Prolong Gold Antifade (Life Technologies) and allowed to cure for 24 h.

For dendritic length and glutamatergic terminal number analysis, images (1024 × 1024 pixels) were obtained using a C2 confocal microscopy system (Nikon) with a 40× oil objective. Images were acquired using equal exposure times between groups in stacks of 4–6 images at 2.0 μm depth intervals and then randomized and renamed to blind analysis. Maximum intensity projections were created using Fiji software. Total dendritic length was obtained by tracing MAP2 expression using the NeuronJ plugin (Meijering et al., 2004). VGLUT1 puncta number were calculated using Intellicount software (Fantuzzo et al., 2017).

Electrophysiology—Whole-cell recordings were performed with patch-clamp amplifiers (MultiClamp 700B amplifier; Molecular Devices) under the control of Clampex 10.3 or 10.5 (Molecular Devices, pClamp, RRID:SCR_011323). Data were acquired at 10 kHz and low-pass filtered at 4 kHz. The series resistance was compensated at 70%, and only cells with series resistances maintained at less than 15 MΩ and stable holding currents of less than 400 pA were analyzed. The pipette resistance was between 2 and 4 MΩ. Standard extracellular solution contained the following (in mM): 140 NaCl, 2.4 KCl, 10 HEPES, 10 glucose, 4 $MgCl_2$, and 2 $CaCl_2$ (pH 7.3, 305 mOsm). Internal solution contained the following: 136 mM K-gluconate, 17.8 mM HEPES, 1 mM EGTA, 0.6 mM $MgCl_2$, 4 mM ATP, 0.3 mM GTP, 12 Mm creatine phosphate, and 50 U/mL phosphocreatine kinase. All experiments were performed at room temperature (22–23°C). Whole-cell recordings were performed on neurons from control and mutant groups in parallel on the same day (day 12–14 *in vitro*) with the experimenter blinded to treatment condition.

For voltage-clamp experiments, neurons were held at −70 mV unless noted. Action potential (AP)-evoked EPSCs were triggered by a 2 ms somatic depolarization to 0 mV. The shape of the evoked response and the effect of receptor antagonists [3 mM kynurenic acid (KYN, Tocris Bioscience) or 20 μM bicuculline (BIC, Tocris Bioscience)] were analyzed to verify the glutamatergic or GABAergic identities of the neurons. Neurons were stimulated at 0.2 Hz in standard external solution to measure basal-evoked synaptic responses. Electrophysiology data were analyzed offline with AxoGraph X software (AxoGraph Scientific, RRID:SCR_014284). To determine the number of releasable SVs onto each neuron, we measured the charge transfer of the transient synaptic current induced by a 5 s application of hypertonic sucrose solution directly onto the neuron and then divided the sucrose charge by the charge of the average miniature event onto the same neuron (Rosenmund and Stevens, 1996).

For current-clamp experiments, the resting membrane potential was measured and then current was injected to achieve a resting membrane potential of −70 mV. KYN was applied to block synaptic responses. Input resistance and membrane time constant were calculated from the steady state and charging transient, respectively, of voltage responses to 0.5 s, 20 pA hyperpolarizing current steps. Membrane capacitance was calculated by dividing the time constant by the input resistance. AP were evoked with 0.5 s, 20 pA depolarizing current steps. AP threshold was defined as the membrane potential at the inflection point of the rising phase of the AP. AP amplitude was defined as the difference in membrane potential

between the AP peak and threshold. The membrane potential values were not corrected for the liquid junction potential.

QUANTIFICATION AND STATISTICAL ANALYSIS

Statistical analysis—All graphical representations of the data were performed in PRISM 9 (GraphPad). For all *in vivo* studies statistical analyses were performed using two parallel methodologies. The first methodology was performed using a mixed-effects model in Stata 15 where the n value was an individual neuron clustered within individual animals (Moen et al., 2016). p-values were then determined by comparing every group to one another using the pwcompare command (Moen et al., 2016). For the second methodology all neurons from an individual animal were averaged and the n value was an individual animal. p values were then calculated using Tukey's or Sidak's multiple comparison test in PRISM 9. For Electrophysiological data were analyzed with SPSS (27.0 Chicago, III (IBM, RRID:SCR_002865). Generalized Estimating Equations were used to test significance for whole cell electrophysiology. Unless otherwise indicated, Mean ± SEM values are calculated using average values of Cre+ and Cre− neurons. Detailed results of statistical analysis are presented in Tables S1–S4.

Supplementary Material

Refer to Web version on PubMed Central for supplementary material.

ACKNOWLEDGMENTS

This work was funded by Autism Speaks predoctoral grant (11857) to K.T. and National Institutes of Health grants R01 (NS110945) to M.W.C. and R01 (MH097949) to B.W.L. This work was also supported by Optical Cellular Imaging Shared Resource at the Geisel School of Medicine at Dartmouth College.

REFERENCES

Angliker N, and Ruegg MA (2013). In vivo evidence for mTORC2-mediated actin cytoskeleton rearrangement in neurons. BioArchitecture 3, 113–118. [PubMed: 24721730]

Antion MD, Hou L, Wong H, Hoeffer CA, and Klann E (2008). mGluR-dependent long-term depression is associated with increased phosphorylation of S6 and synthesis of elongation factor 1A but remains expressed in S6K-deficient mice. Mol. Cell Biol 28, 2996–3007. [PubMed: 18316404]

Cardamone M, Flanagan D, Mowat D, Kennedy SE, Chopra M, and Lawson JA (2014). Mammalian target of rapamycin inhibitors for intractable epilepsy and subependymal giant cell astrocytomas in tuberous sclerosis complex. J. Pediatr 164, 1195–1200. [PubMed: 24518170]

Chen CJ, Sgritta M, Mays J, Zhou H, Lucero R, Park J, Wang IC, Park JH, Kaipparettu BA, Stoica L, et al. (2019). Therapeutic inhibition of mTORC2 rescues the behavioral and neurophysiological abnormalities associated with Pten-deficiency. Nat. Med 25, 1684–1690. [PubMed: 31636454]

Chen Y, Huang WC, Séjourné J, Clipperton-Allen AE, and Page DT (2015). Pten mutations alter brain growth trajectory and allocation of cell types through elevated beta-catenin signaling. J. Neurosci 35, 10252–10267. [PubMed: 26180201]

Conti S, Condò M, Posar A, Mari F, Resta N, Renieri A, Neri I, Patrizi A, and Parmeggiani A (2012). Phosphatase and tensin homolog (PTEN) gene mutations and autism: literature review and a case report of a patient with Cowden syndrome, autistic disorder, and epilepsy. J. Child Neurol 27, 392–397. [PubMed: 21960672]

Dunlop EA, and Tee AR (2014). mTOR and autophagy: a dynamic relationship governed by nutrients and energy. Semin. Cell Dev. Biol 36, 121–129. [PubMed: 25158238]

Fantuzzo JA, Mirabella VR, Hamod AH, Hart RP, Zahn JD, and Pang ZP (2017). Intellicount: high-throughput quantification of fluorescent synaptic protein puncta by machine learning. eNeuro 4. ENEURO.0219-17.2017.

Fricano CJ, Despenza T Jr., Frazel PW, Li M, O'Malley AJ, Westbrook GL, and Luikart BW (2014). Fatty acids increase neuronal hypertrophy of Pten knockdown neurons. Front. Mol. Neurosci 7, 30. [PubMed: 24795563]

Fricano-Kugler CJ, Williams MR, Salinaro JR, Li M, and Luikart B (2016). Designing, packaging, and delivery of high titer CRISPR retro and lentiviruses via stereotaxic injection. J. Vis. Exp 23, 53783.

Getz SA, DeSpenza T Jr., Li M, and Luikart BW (2016). Rapamycin prevents, but does not reverse, aberrant migration in Pten knockout neurons. Neurobiol. Dis 93, 12–20. [PubMed: 26992888]

Godale CM, Parkins EV, Gross C, and Danzer SC (2022). Impact of raptor and rictor deletion on hippocampal pathology following status epilepticus. J. Mol. Neurosci 72, 1243–1258. [PubMed: 35618880]

Hsu PP, Kang SA, Rameseder J, Zhang Y, Ottina KA, Lim D, Peterson TR, Choi Y, Gray NS, Yaffe MB, et al. (2011). The mTOR-regulated phosphoproteome reveals a mechanism of mTORC1-mediated inhibition of growth factor signaling. Science 332, 1317–1322. [PubMed: 21659604]

Huang W, Zhu PJ, Zhang S, Zhou H, Stoica L, Galiano M, Krnjević K, Roman G, and Costa-Mattioli M (2013). mTORC2 controls actin polymerization required for consolidation of long-term memory. Nat. Neurosci 16, 441–448. [PubMed: 23455608]

Kang SA, Pacold ME, Cervantes CL, Lim D, Lou HJ, Ottina K, Gray NS, Turk BE, Yaffe MB, and Sabatini DM (2013). mTORC1 phosphorylation sites encode their sensitivity to starvation and rapamycin. Science 341, 1236566. [PubMed: 23888043]

Karalis V, Caval-Holme F, and Bateup HS (2022). Raptor downregulation rescues neuronal phenotypes in mouse models of Tuberous Sclerosis Complex. Nat. Commun 13, 4665. [PubMed: 35945201]

Klein S, Sharifi-Hannauer P, and Martinez-Agosto JA (2013). Macrocephaly as a clinical indicator of genetic subtypes in autism. Autism Res 6, 51–56. [PubMed: 23361946]

Kwon CH, Luikart BW, Powell CM, Zhou J, Matheny SA, Zhang W, Li Y, Baker SJ, and Parada LF (2006). Pten regulates neuronal arborization and social interaction in mice. Neuron 50, 377–388. [PubMed: 16675393]

Laplante M, and Sabatini DM (2009). mTOR signaling at a glance. J. Cell Sci 122, 3589–3594. [PubMed: 19812304]

Laplante M, and Sabatini DM (2012). mTOR signaling in growth control and disease. Cell 149, 274–293. [PubMed: 22500797]

Liu GY, and Sabatini DM (2020). mTOR at the nexus of nutrition, growth, ageing and disease. Nat. Rev. Mol. Cell Biol 21, 183–203. [PubMed: 31937935]

Liu P, Gan W, Chin YR, Ogura K, Guo J, Zhang J, Wang B, Blenis J, Cantley LC, Toker A, et al. (2015). PtdIns(3, 4, 5)P3-dependent activation of the mTORC2 kinase complex. Cancer Discov 5, 1194–1209. [PubMed: 26293922]

Luikart BW, Bensen AL, Washburn EK, Perederiy JV, Su KG, Li Y, Kernie SG, Parada LF, and Westbrook GL (2011a). miR-132 mediates the integration of newborn neurons into the adult dentate gyrus. PLoS One 6, e19077. [PubMed: 21611182]

Luikart BW, Schnell E, Washburn EK, Bensen AL, Tovar KR, and Westbrook GL (2011b). Pten knockdown in vivo increases excitatory drive onto dentate granule cells. J. Neurosci 31, 4345–4354. [PubMed: 21411674]

McCabe MP, Cullen ER, Barrows CM, Shore AN, Tooke KI, Laprade KA, Stafford JM, and Weston MC (2020). Genetic inactivation of mTORC1 or mTORC2 in neurons reveals distinct functions in glutamatergic synaptic transmission. Elife 9, e51440. [PubMed: 32125271]

Meijering E, Jacob M, Sarria JCF, Steiner P, Hirling H, and Unser M (2004). Design and validation of a tool for neurite tracing and analysis in fluorescence microscopy images. Cytometry A 58, 167–176. [PubMed: 15057970]

Mizuguchi M, Ikeda H, Kagitani-Shimono K, Yoshinaga H, Suzuki Y, Aoki M, Endo M, Yonemura M, and Kubota M (2019). Everolimus for epilepsy and autism spectrum disorder in tuberous sclerosis complex: EXIST-3 substudy in Japan. Brain Dev 41, 1–10. [PubMed: 30060984]

Moen EL, Fricano-Kugler CJ, Luikart BW, and O'Malley AJ (2016). Analyzing clustered data: why and how to account for multiple observations nested within a study participant? PLoS One 11, e0146721. [PubMed: 26766425]

Perederiy JV, Luikart BW, Washburn EK, Schnell E, and Westbrook GL (2013). Neural injury alters proliferation and integration of adult-generated neurons in the dentate gyrus. J. Neurosci 33, 4754–4767. [PubMed: 23486947]

Peterson TR, Laplante M, Thoreen CC, Sancak Y, Kang SA, Kuehl WM, Gray NS, and Sabatini DM (2009). DEPTOR is an mTOR inhibitor frequently overexpressed in multiple myeloma cells and required for their survival. Cell 137, 873–886. [PubMed: 19446321]

Rodriguez A, Ehlenberger DB, Dickstein DL, Hof PR, and Wearne SL (2008). Automated three-dimensional detection and shape classification of dendritic spines from fluorescence microscopy images. PLoS One 3, e1997. [PubMed: 18431482]

Rosenmund C, and Stevens CF (1996). Definition of the readily releasable pool of vesicles at hippocampal synapses. Neuron 16, 1197–1207. [PubMed: 8663996]

Sabatini DM, Erdjument-Bromage H, Lui M, Tempst P, and Snyder SH (1994). RAFT1: a mammalian protein that binds to FKBP12 in a rapamycin-dependent fashion and is homologous to yeast TORs. Cell 78, 35–43. [PubMed: 7518356]

Sage D, Donati L, Soulez F, Fortun D, Schmit G, Seitz A, Guiet R, Vonesch C, and Unser M (2017). DeconvolutionLab2: an open-source software for deconvolution microscopy. Methods 115, 28–41. [PubMed: 28057586]

Santos VR, Pun RYK, Arafa SR, LaSarge CL, Rowley S, Khademi S, Bouley T, Holland KD, Garcia-Cairasco N, and Danzer SC (2017). PTEN deletion increases hippocampal granule cell excitability in male and female mice. Neurobiol. Dis 108, 339–351. [PubMed: 28855130]

Sarbassov DD, Ali SM, Sengupta S, Sheen JH, Hsu PP, Bagley AF, Markhard AL, and Sabatini DM (2006). Prolonged rapamycin treatment inhibits mTORC2 assembly and Akt/PKB. Mol. Cell 22, 159–168. [PubMed: 16603397]

Sarbassov DD, Guertin DA, Ali SM, and Sabatini DM (2005). Phosphorylation and regulation of Akt/PKB by the rictor-mTOR complex. Science 307, 1098–1101. [PubMed: 15718470]

Sarn N, Jaini R, Thacker S, Lee H, Dutta R, and Eng C (2021). Cytoplasmic-predominant Pten increases microglial activation and synaptic pruning in a murine model with autism-like phenotype. Mol. Psychiatry 26, 1458–1471. [PubMed: 32055008]

Satterstrom FK, Kosmicki JA, Wang J, Breen MS, De Rubeis S, An JY, Peng M, Collins R, Grove J, Klei L, et al. (2020). Large-scale exome sequencing study implicates both developmental and functional changes in the neurobiology of autism. Cell 180, 568–584.e23. [PubMed: 31981491]

Saxton RA, and Sabatini DM (2017). mTOR signaling in growth, metabolism, and disease. Cell 169, 361–371.

Sengupta S, Peterson TR, Laplante M, Oh S, and Sabatini DM (2010). mTORC1 controls fasting-induced ketogenesis and its modulation by ageing. Nature 468, 1100–1104. [PubMed: 21179166]

Skelton PD, Frazel PW, Lee D, Suh H, and Luikart BW (2019). Pten loss results in inappropriate excitatory connectivity. Mol. Psychiatry 24, 1627–1640. [PubMed: 30967683]

Skelton PD, Poquerusse J, Salinaro JR, Li M, and Luikart BW (2020). Activity-dependent dendritic elaboration requires Pten. Neurobiol. Dis 134, 104703. [PubMed: 31838155]

Takei N, and Nawa H (2014). mTOR signaling and its roles in normal and abnormal brain development. Front. Mol. Neurosci 7, 28. [PubMed: 24795562]

Takei N, Inamura N, Kawamura M, Namba H, Hara K, Yonezawa K, and Nawa H (2004). Brain-derived neurotrophic factor induces mammalian target of rapamycin-dependent local activation of translation machinery and protein synthesis in neuronal dendrites. J. Neurosci 24, 9760–9769. [PubMed: 15525761]

Tariq K, and Luikart BW (2021). Striking a balance: PIP_2 and PIP_3 signaling in neuronal health and disease. Explor. Neuroprot. Ther 1, 86–100.

Tzatsos A (2009). Raptor binds the SAIN (Shc and IRS-1 NPXY binding) domain of insulin receptor substrate-1 (IRS-1) and regulates the phosphorylation of IRS-1 at Ser-636/639 by mTOR. J. Biol. Chem 284, 22525–22534. [PubMed: 19561084]

Vogt D, Cho KKA, Lee AT, Sohal VS, and Rubenstein JLR (2015). The parvalbumin/somatostatin ratio is increased in Pten mutant mice and by human PTEN ASD alleles. Cell Rep 11, 944–956. [PubMed: 25937288]

Waite KA, and Eng C (2002). Protean PTEN: form and function. Am. J. Hum. Genet 70, 829–844. [PubMed: 11875759]

Weston MC, Chen H, and Swann JW (2012). Multiple roles for mammalian target of rapamycin signaling in both glutamatergic and GABAergic synaptic transmission. J. Neurosci 32, 11441–11452. [PubMed: 22895726]

Williams MR, DeSpenza T Jr., Li M, Gulledge AT, and Luikart BW (2015). Hyperactivity of newborn Pten knock-out neurons results from increased excitatory synaptic drive. J. Neurosci 35, 943–959. [PubMed: 25609613]

Zhou J, Blundell J, Ogawa S, Kwon CH, Zhang W, Sinton C, Powell CM, and Parada LF (2009). Pharmacological inhibition of mTORC1 suppresses anatomical, cellular, and behavioral abnormalities in neural-specific Pten knock-out mice. J. Neurosci 29, 1773–1783. [PubMed: 19211884]

Zhu G, Chow LML, Bayazitov IT, Tong Y, Gilbertson RJ, Zakharenko SS, Solecki DJ, and Baker SJ (2012). Pten deletion causes mTorc1-dependent ectopic neuroblast differentiation without causing uniform migration defects. Development 139, 3422–3431. [PubMed: 22874917]

Highlights

- *Pten* KO results in increased neuronal growth and excitatory synapse function
- Pharmacological inhibition of mTOR prevents morphological changes in *Pten* KO
- *Raptor* KO rescues morphological and synaptic phenotypes of *Pten* KO
- Downstream mTORC1 function is necessary for neuronal growth and synapse formation

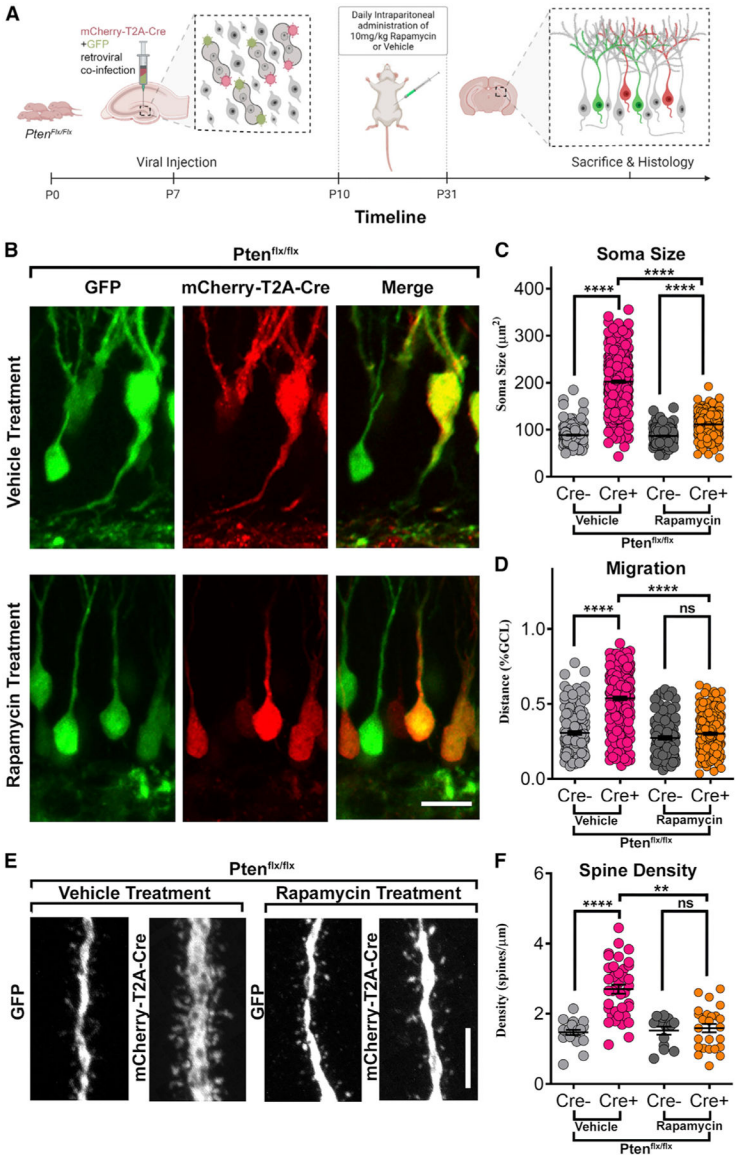

Figure 1. Rapamycin treatment rescues *Pten* KO-mediated somal hypertrophy, aberrant migration, and increased spine density

(A) Schematic of experimental setup. Retroviruses encoding a fluorophore only (GFP) or a fluorophore and Cre recombinase (mCherry-T2A-Cre) were co-injected into dentate gyrus of *Pten*$^{flx/flx}$ animals at postnatal day 7 (P7). Rapamycin (10 mg/kg of body weight) or vehicle was administered intraperitoneally from P10 to P31 daily. At P31, animals were perfused, and immunohistochemistry of hippocampal slices was performed for subsequent imaging and analysis.

(B) Top panel shows representative images of vehicle-treated immunolabeled granule neurons from *Pten*$^{flx/flx}$ animals, while bottom panel shows representative images of rapamycin-treated immunolabeled granule neurons from *Pten*$^{flx/flx}$ animals (scale bar represents 20 μm).

(C) *Pten* KO-mediated somal hypertrophy was completely rescued with rapamycin treatment, when compared with vehicle-treated *Pten* KO granule neurons.

(D) Rapamycin treatment of *Pten* KO granule neurons completely rescued the farther migration of vehicle-treated *Pten* KO granule neurons in the granule cell layer (GCL).
(E) Representative images for spine density analysis (scale bar represents 5 μm).
(F) The increased spine density of vehicle-treated *Pten* KO granule neurons was rescued by rapamycin treatment. The mixed-effects model in STATA was performed to determine p value (*$p < 0.05$, **$p < 0.01$, ***$p < 0.001$, ****$p < 0.0001$). See Tables S1A–S1C for detailed statistics and quantitative results.

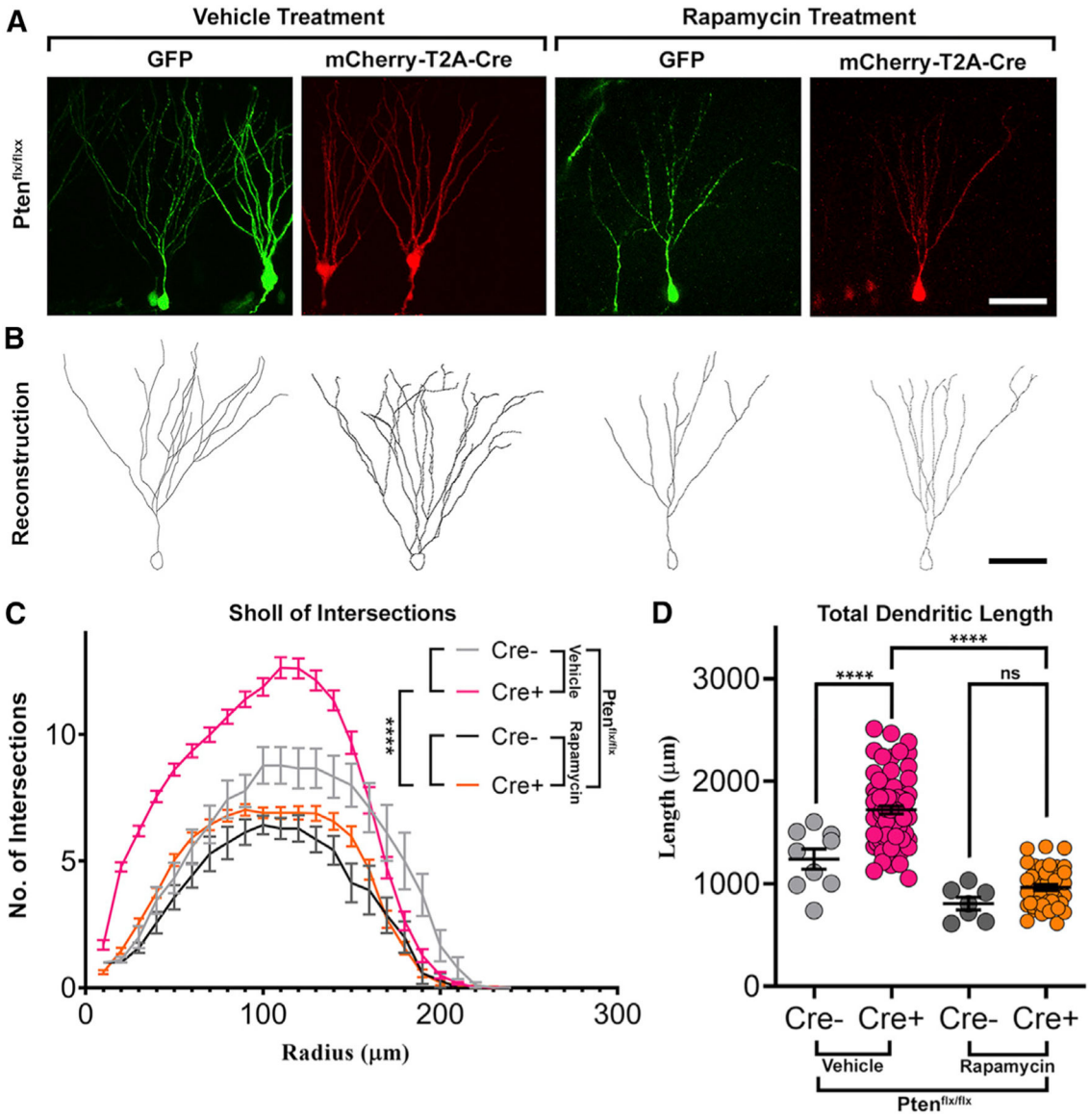

Figure 2. Rapamycin treatment rescues *Pten* KO-mediated dendritic overgrowth

Retroviruses encoding a fluorophore only (GFP) or a fluorophore and Cre recombinase (mCherry-T2A-Cre) were co-injected into dentate gyrus of *Pten*$^{flx/flx}$ animals at postnatal day 7 (P7). Rapamycin (10 mg/kg of body weight) or vehicle was administered intraperitoneally from P10 to P31 daily. At P31, animals were perfused, and immunohistochemistry of hippocampal slices was performed for dendritic arbor reconstruction.

(A) Representative images of vehicle- or rapamycin-treated immunolabeled granule neurons from *Pten*$^{flx/flx}$ animals (scale bar represents 50 μm).

(B) 2D reconstructions of neurons in (A) (scale bar represents 50 μm).

(C) The increase in Sholl analysis of intersections of vehicle-treated *Pten* KO granule neurons was rescued by rapamycin treatment.

(D) Rapamycin treatment rescued the increase in total dendritic length of vehicle-treated *Pten* KO granule neurons. The mixed-effects model in STATA was performed to determine p value (*$p < 0.05$, **$p < 0.01$, ***$p < 0.001$, ****$p < 0.0001$). See Tables S1F–S1G for statistics and quantitative results.

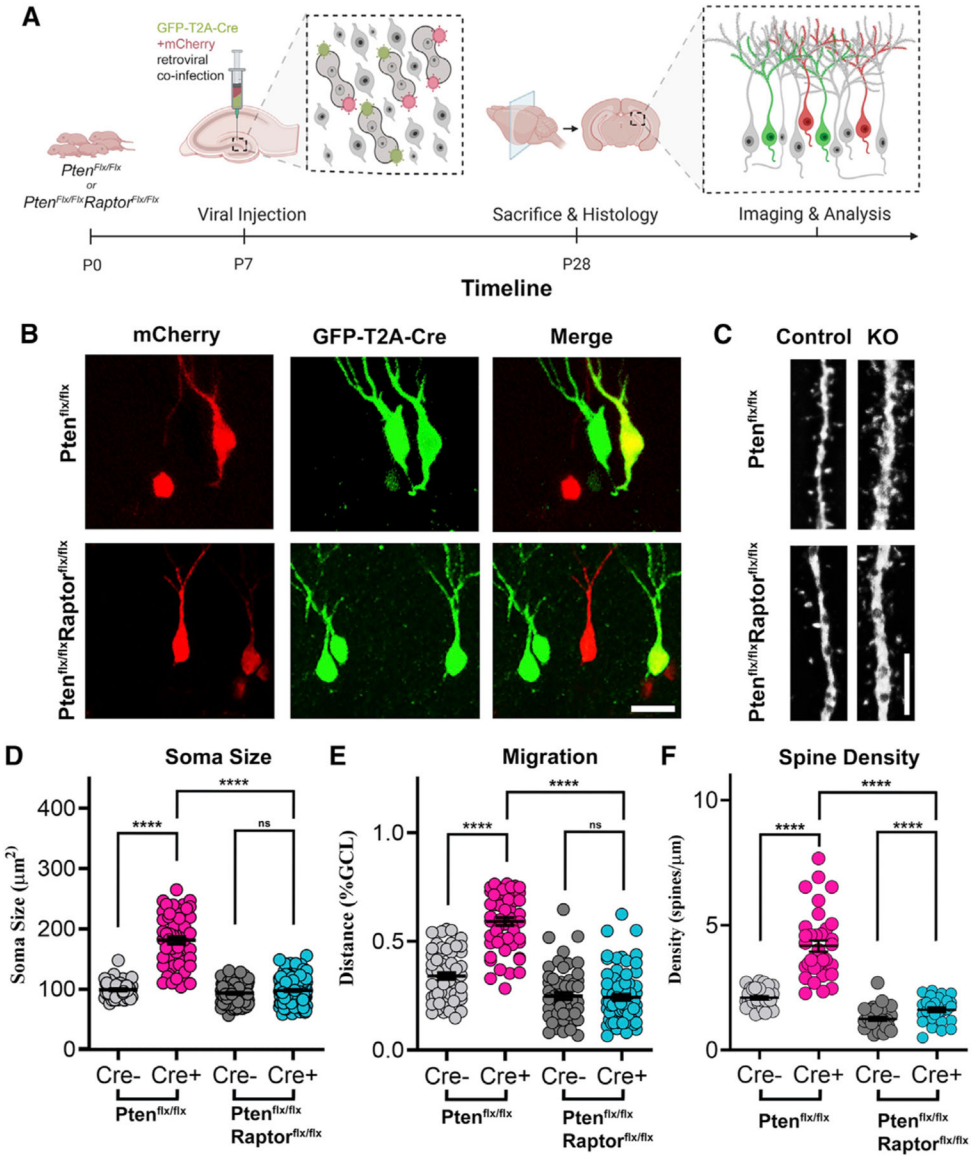

Figure 3. Genetic disruption of mTORC1 rescues *Pten* KO-mediated somal hypertrophy, aberrant migration, and increased spine density

(A) Schematic of experimental setup. Retroviruses encoding a fluorophore only (mCherry) or a fluorophore and Cre recombinase (GFP-T2A-Cre) were co-injected into dentate gyrus of either *Pten*$^{flx/flx}$, or *Pten*$^{flx/flx}$*Raptor*$^{flx/flx}$ animals at postnatal day 7 (P7). At postnatal day 28 (P28), animals were perfused, and immunohistochemistry was performed for subsequent imaging and analysis.

(B) Top panels show representative images of immunolabeled granule neurons from *Pten*$^{flx/flx}$ animals, while bottom panels show representative images of immunolabeled granule neurons from *Pten*$^{flx/flx}$*Raptor*$^{flx/flx}$ animals, for soma size and migration analysis (scale bar represents 20 μm).

(C) Representative images for spine density analysis (scale bar represents 5 μm).

(D) *Pten* KO-mediated somal hypertrophy was completely rescued in *Pten* and *Raptor* DKO granule neurons.

(E) The farther migration of *Pten* KO granule neurons in the granule cell layer (GCL) was completely rescued in *Pten* and *Raptor* DKO granule neurons.
(F) The *Pten* KO-mediated increase in spine density was completely rescued in *Pten* and *Raptor* DKO granule neurons. The mixed-effects model in STATA was performed to determine p value (*$p < 0.05$, **$p < 0.01$, ***$p < 0.001$, ****$p < 0.0001$). See Tables S1A–S1C for statistical and quantitative results.

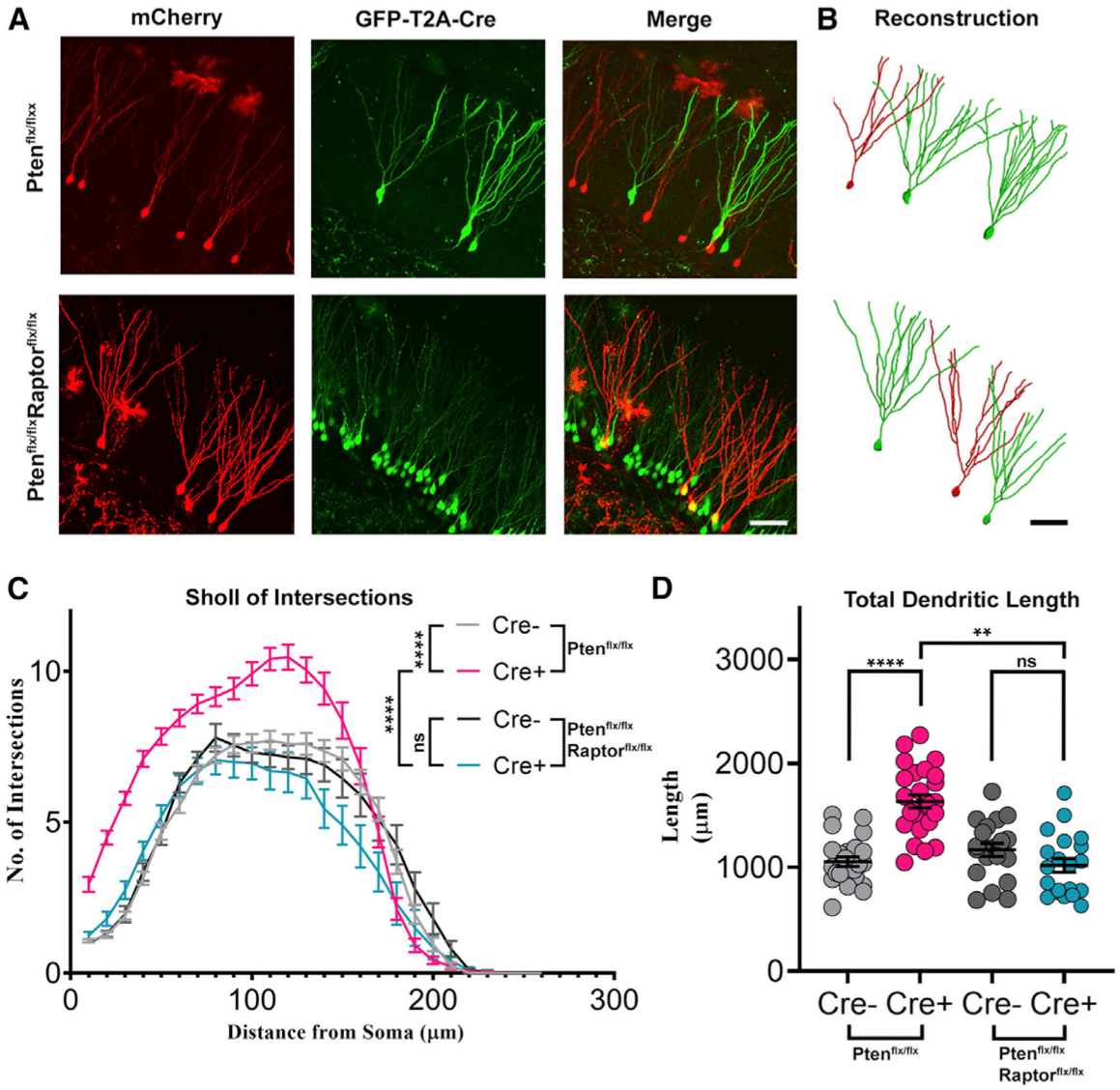

Figure 4. Genetic disruption of mTORC1 rescues *Pten* KO-mediated dendritic overgrowth

Hippocampal dentate gyrus of *Pten*$^{flx/flx}$ or *Pten*$^{flx/flx}$ *Raptor*$^{flx/flx}$ animals were co-injected with fluorophore only (mCherry) retrovirus or fluorophore and Cre (GFP-T2A-Cre) retrovirus at P7. Animals were perfused at P28 for subsequent immunohistochemistry and reconstruction of dendritic arbor.

(A) Top panels show representative images of immunolabeled granule neurons from *Pten*$^{flx/flx}$ animals, while bottom panels show representative images of immunolabeled granule neurons from *Pten*$^{flx/flx}$*Raptor*$^{flx/flx}$ animal (scale bar represents 50 μm).

(B) 3D reconstructions of neurons in (A) (scale bar represents 50 μm).

(C) *Pten* and *Raptor* DKO completely rescues the increase in Sholl of intersections of *Pten* KO granule neurons.

(D) Increased total dendritic length of *Pten* KO granule neurons was rescued in *Pten* and *Raptor* DKO granule neurons. The mixed-effects model in STATA was performed to

determine p value (*p < 0.05, **p < 0.01, ***p < 0.001, ****p < 0.0001). See Tables S1F–S1G for statistics and quantitative results.

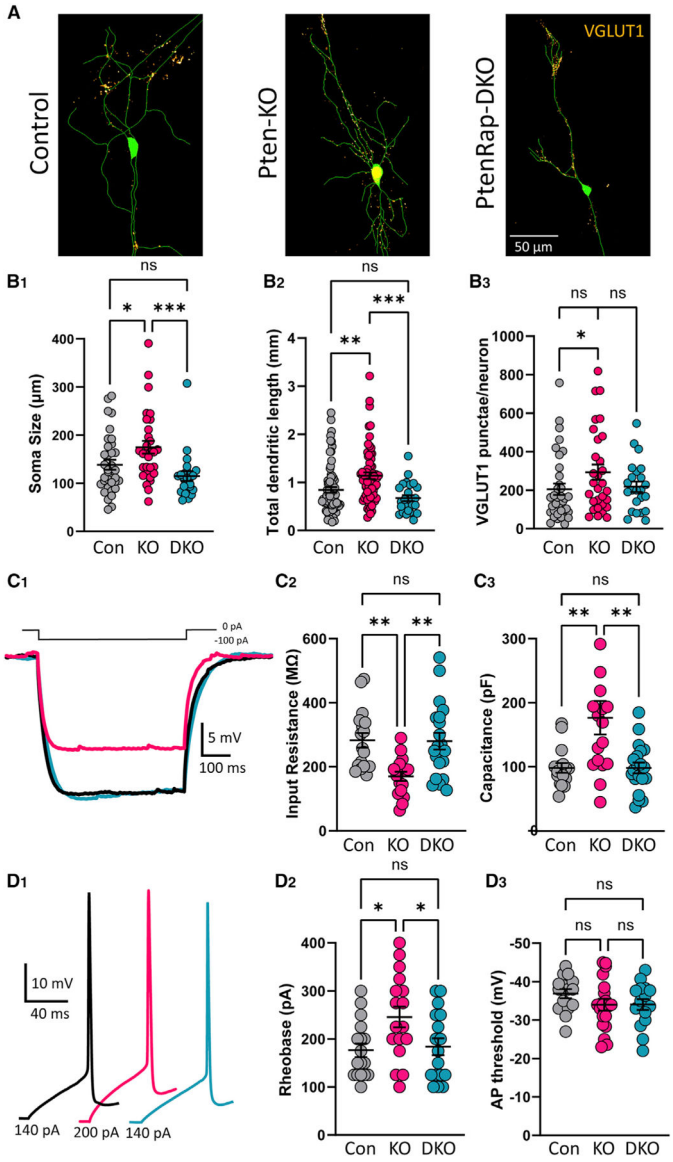

Figure 5. Genetic disruption of mTORC1 rescues *Pten* KO-mediated hypertrophy and membrane hypoexcitability in single neuron cultures

(A) Representative images showing fluorescence intensity in an orange color look up table (LUT) from VGLUT1 immunostaining superimposed on a tracing of the cell body and dendrites of a control (left), *Pten* KO (center), and *PtenRaptor* DKO (right) neuron. (B) The soma size, dendritic length, and number of VGLUT1-positive puncta of *Pten* KO neurons is increased relative to control and decreased in *PtenRaptor* DKO neurons. (C_1) Example current-clamp traces of the membrane voltage (Vm) response of control (black), *Pten* KO (magenta), and *PtenRaptor* DKO (cyan) to a −100-pA, 500-ms current step. (C_2) The input resistance and capacitance changes caused by *Pten* KO, calculated from the negative current injections, is normalized in *PtenRaptor* DKO neurons. (For dot plots, each dot represents the data point from one neuron.) Generalized estimating equations in SPSS were used for statistical analysis. (*$p < 0.05$, **$p < 0.01$, ***$p < 0.001$). See Table S2 for statistics and quantitative data.

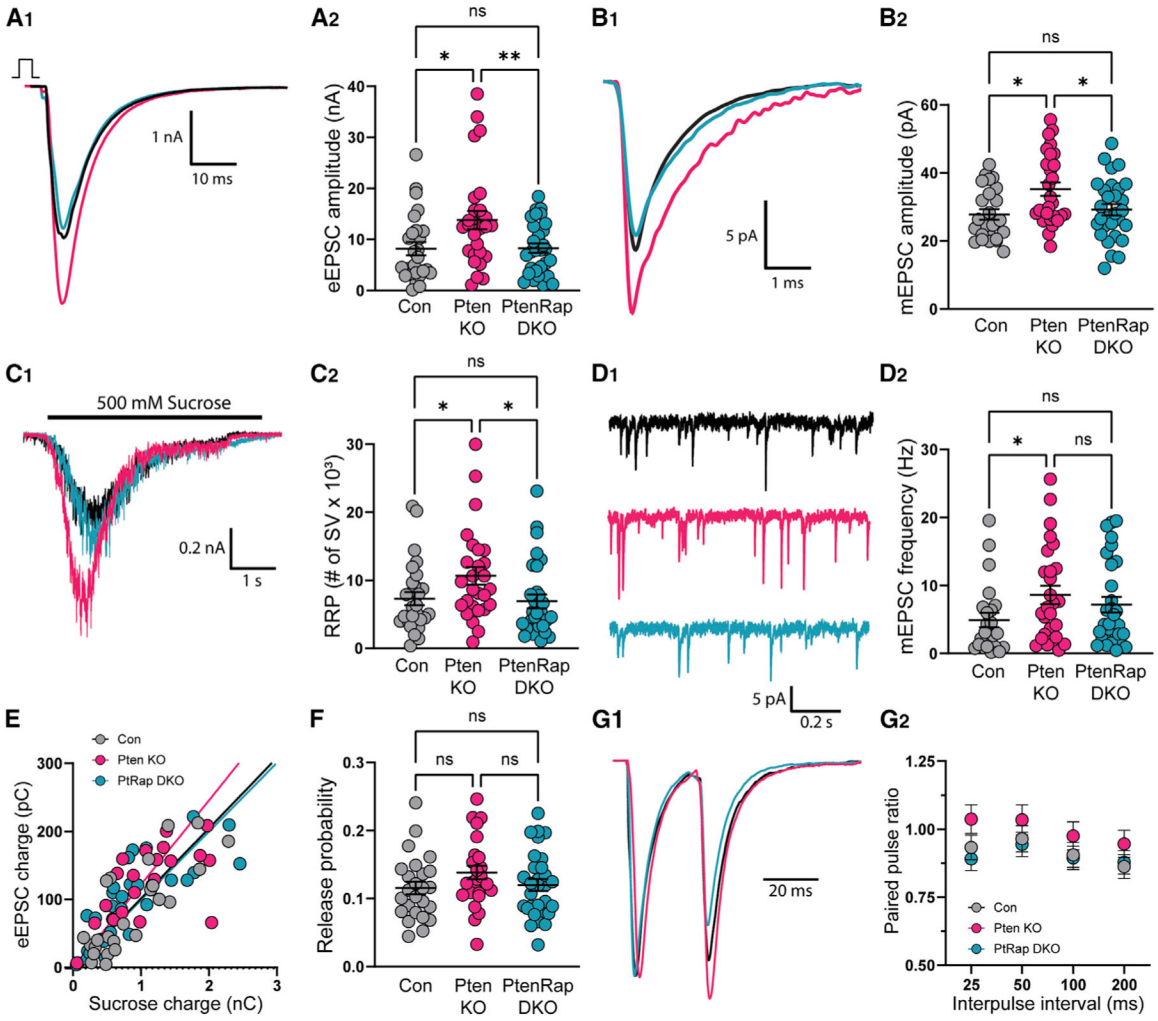

Figure 6. Genetic disruption of mTORC1 rescues *Pten* KO-mediated increases in excitatory synaptic transmission

(A) Representative traces (A_1) and summary data (A_2) of EPSCs evoked by a 2-ms depolarization from control (black), *Pten* KO (magenta), and *PtenRaptor* DKO (cyan) neurons.

(B) Representative traces (B_1) and summary data (B_2) of miniature EPSCs recorded in TTX from control (black), *Pten* KO (magenta), and *PtenRaptor* DKO (cyan) neurons.

(C) Representative traces (C_1) of the current response to 500 mM sucrose application and summary data (C_2) of the number of synaptic vesicles in the readily releasable pool.

(D) Representative traces (D_1) of miniature EPSCs recorded in TTX and summary data (D_2) of the mEPSC frequency.

(E) Scatterplot of eEPSC charge versus RRP charge. Solid lines represent regression lines. The average release fraction is given by the slopes of the regression lines.

(F) Vesicular release probability calculated by dividing sucrose charge by eEPSC charge for each neuron.

(G) Example traces (G_1) of two eEPSC separated by 25 ms and normalized to the peak of the first eEPSC, along with summary data (G_2) showing mean ± SEM for each genotype

and interpulse interval. For dot plots, each dot represents the data point from one neuron. Generalized estimating equations in SPSS were used for statistical analysis. (*$p < 0.05$, **$p < 0.01$). See Table S2 for statistics and quantitative data.

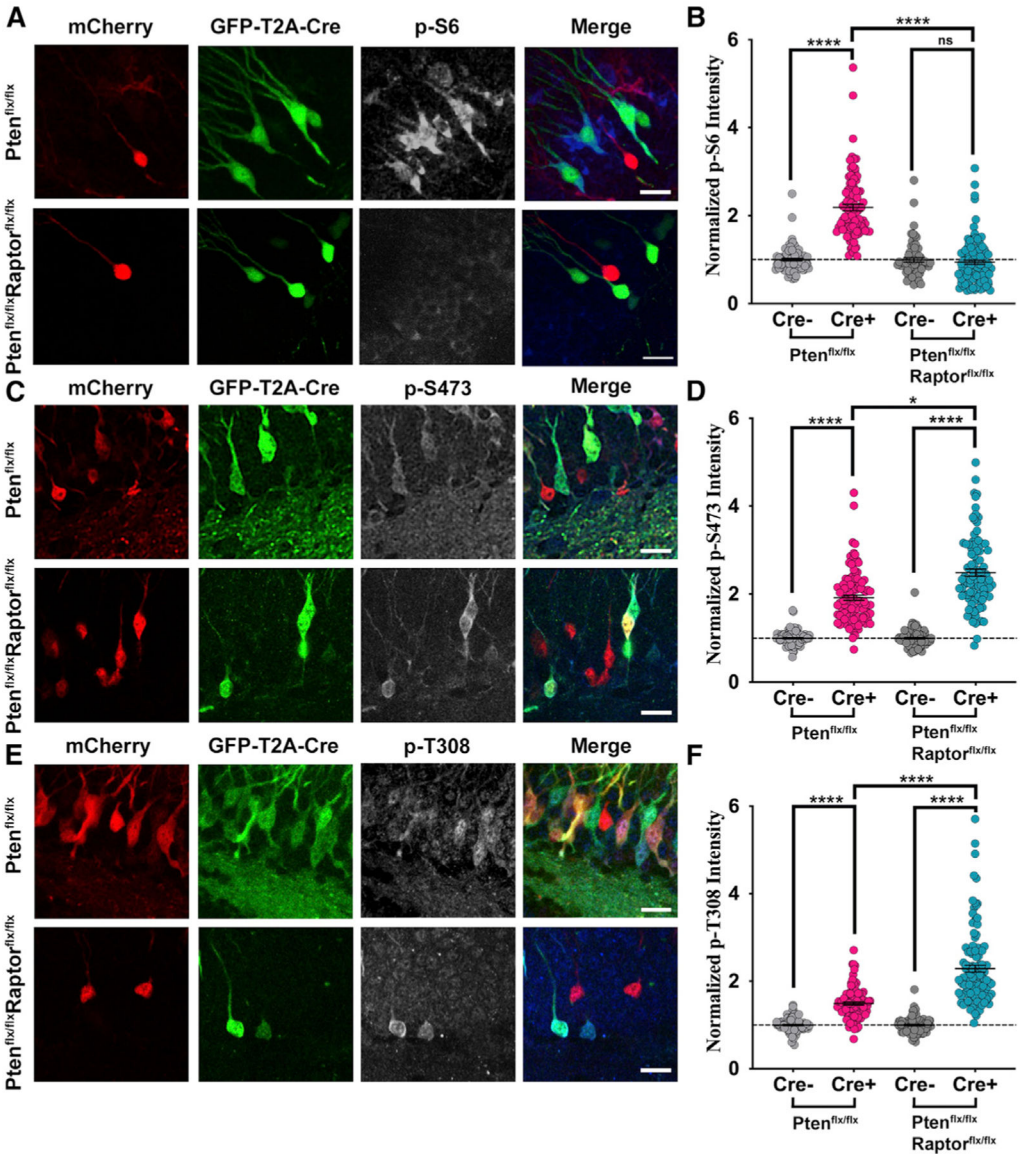

Figure 7. Genetic KO of *Raptor* leads to loss of mTORC1 activity in *Pten* KO granule neurons

(A) Top panel shows representative images of immunolabeled granule neurons from *Pten*$^{flx/flx}$ animals stained for phosphorylation of S6 (pS6), while bottom panel shows representative images of immunolabeled granule neurons from *Pten*$^{flx/flx}$ *Raptor*$^{flx/flx}$ animals stained for pS6 (scale bar represents 20 μm).

(B) The relative fluorescence intensity of pS6 was quantified as a readout of mTORC1 activity. *Pten* KO neurons showed an increase in normalized pS6 intensity, indicating increased mTORC1 activity. The increase in pS6 intensity was completely rescued in *Pten* and *Raptor* DKO neurons, indicating loss of mTORC1 activity.

(C) Top panel shows representative images of immunolabeled granule neurons from *Pten*$^{flx/flx}$ animals stained for phosphorylation of AKT threonine 308 (pT308), while bottom panel shows representative images of immunolabeled granule neurons from *Pten*$^{flx/flx}$*Raptor*$^{flx/flx}$ animals stained for pAKT T308 (scale bar represents 20 μm).

(D) The relative fluorescence intensity of pAKT T308 was quantified as a readout of PDK1 activity. *Pten* KO neurons showed increased normalized pAKT T308 intensity compared with control, indicating greater PDK1 activity; however, *Pten* and *Raptor* DKO neurons demonstrated even greater pAKT T308 intensity, suggesting PDK1 activity was greater in the absence of both *Pten* and *Raptor* than solely *Pten*.
(E) Top panel shows representative images of immunolabeled granule neurons from $Pten^{flx/flx}$ animals stained for phosphorylation of AKT serine 473 (pS473), while bottom panel shows representative images of immunolabeled granule neurons from $Pten^{flx/flx}Raptor^{flx/flx}$ animals stained for pAKT S473 (scale bar represents 20 μm).
(F) The relative fluorescence intensity of pAKT S473 was quantified as a readout of mTORC2 activity. *Pten* KO neurons demonstrated an increase in normalized pAKT S473 intensity compared with control, indicating elevated mTORC2 activity; however, *Pten* and *Raptor* DKO neurons showed an even greater increase in pAKT S473 intensity, suggesting mTORC2 activity was significantly higher in the absence of both *Pten* and *Raptor* than solely *Pten*. The mixed-effects model in STATA was performed to determine p value (*$p < 0.05$, **$p < 0.01$, ***$p < 0.001$, ****$p < 0.0001$). See Table S3 for statistics and quantitative data.

KEY RESOURCES TABLE

REAGENT or RESOURCE	SOURCE	IDENTIFIER
Antibodies		
Chicken anti-GFP	abcam	Cat# 13970; RRID: AB_300798
Rabbit anti-mCherry	abcam	Cat# 167453; RRID: AB_2571870
Mouse anti-mCherry	TaKaRa	Cat# 632543; RRID: AB_2307319
Rabbit anti-phospho-S6 S235/236	Cell Signaling	Cat# 4858; RRID: AB_916156
Rabbit anti-phospho-AKT-Thr308	Cell Signaling	Cat# 13038; RRID: AB_2629447
Rabbit anti-phospho-AKT-Ser473	Cell Signaling	Cat# 9271; RRID: AB_329825
Mouse anti-MAP2	Synaptic Systems	Cat# 188 011; RRID: AB_2147096
Rabbit anti-VGLUT1	Synaptic Systems	Cat# 135 302; RRID: AB_887877
Bacterial and virus strains		
pRubiC-T2A-cre	Addgene	RRID: Addgene_66692
pRubiG-T2A-cre	Addgene	RRID: Addgene_66693
pRubiG	Addgene	RRID: Addgene_66696
pRubiC	Addgene	RRID: Addgene_66700
Experimental models: Organisms/strains		
Pten $^{flx/flx}$	Jackson Laboratory	RRID: IMSR_JAX:006440
Raptor $^{flx/flx}$	Jackson Laboratory	RRID: IMSR_JAX:013188
Deposited Data		
Neuronal Reconstructions	NeuroLucidaB	Neuromorpho.org: Luikart Archive